Synthesis and Characterization of Polyimide–Silica Nanocomposites Using Novel Fluorine-Modified Silica Nanoparticles

Te-Cheng Mo,[1] Hong-Wen Wang,[2] San-Yan Chen,[1] Rui-Xuan Dong,[2] Chien-Hung Kuo,[2] Yun-Chieh Yeh[2]

[1]*Department of Materials Science and Engineering, National Chiao-Tung University, Hsinchu 30049, Taiwan, Republic of China*
[2]*Department of Chemistry, Chung-Yuan Christian University, Chungli 32023, Taiwan, Republic of China*

Received 28 September 2005; accepted 16 October 2006
DOI 10.1002/app.25763
Published online in Wiley InterScience (www.interscience.wiley.com).

ABSTRACT: Polyimide–silica nanocomposites were synthesized with 4,4′-oxydianiline, 4,4′-(4,4′-isopropylidenediphenoxy)bis(phthalic anhydride), and fluorine-modified silica nanoparticles. Fluorinated precursors such as 4″,4‴-(hexafluoroisopropylidene)bis(4-phenoxyaniline) (6FBPA) and 4,4′-(hexafluoroisopropylindene)diphenol (BISAF) were employed to modify the surface of the silica nanoparticles. The microstructures and thermal, mechanical, and dielectric properties of the polyimide–silica nanocomposites were investigated. An improvement in the thermal stability and storage modulus of the polyimide nanocomposites due to the addition of the modified silica nanoparticles was observed. The microstructures of the polyimide–silica nanocomposites containing 6FBPA-modified silica exhibited more uniformity than those of the nanocomposites containing BISAF-modified silica. The dielectric constants of the polyimide were considerably reduced by the incorporation of pristine silica or 6FBPA-modified silica but not BISAF-modified silica. The addition of a modifier with higher fluorine contents did not ensure a lower dielectric constant. The uniformity of the silica distribution, manipulated by the reactivity of the modifier, played an important role in the reduction of the dielectric constant. Using 6FBPA-modified silica nanoparticles demonstrated an effective way of synthesizing low-dielectric-constant polyimide–silica nanocomposites. J Appl Polym Sci 104: 882–890, 2007

Key words: composites; dielectric properties; nanocomposites; polyimides; silicas

INTRODUCTION

Organic–inorganic hybrid nanocomposites have been recognized as a new class of advanced materials because of their versatile competence in synthesis, processing, and tunable properties. Hybrid nanocomposites have important applications in modern microelectronics because of their insulating properties and low dielectric constant (k).[1–3] Polyimide (PI) materials are widely used as high-performance polymers in advanced technologies because of their low water absorption, low thermal expansion coefficients, low k values, and high thermal stability.[4–7] PI is formed by the imidization of poly(amic acid), which can be derived from many kinds of diamines and dianhydrides.[7–10] PI–inorganic nanocomposites for low-k applications have been intensively studied in recent years.[8–32] Studies of pristine PI and fluorinated PI have revealed that the major characteristics for low k values are large free volumes, high fluorine contents, low polarizability, and symmetric fluorinated groups in the polymer structure.[8–20] In general, low-k PI can be achieved with fluorinated starting monomers. However, fluorinated monomers are expensive. To reduce the use of fluorinated monomers in PI nanocomposites while k is kept relatively low is desirable. The creation of nanofoam within a PI matrix is an alternative way to achieve low k values, but it suffers from weak mechanical properties.[20–22] PI hybridized with an organosilicon nanophase offers an opportunity for low k values and good mechanical strength.[23–25] Yen and Chen[26] prepared PI–silica hybrid films through intrachain and interchain bonding. The incorporation of 6.5–7.99 wt % nanosized silica produced PI hybrid films with enhanced thermal stability and low k values in the range of 2.85–3.73. It is also known that hybridizing PI with inorganic materials such as clay and silica is an effective approach to low-k thin-film dielectric layers.[27–31] However, increasing k by the addition of silica ceramic nanoparticles has also been reported.[32]

Nanosilica is expected to enhance the thermal and mechanical properties of a polymer matrix because the nature and behavior of the filler–polymer interface will exert a major influence on the macroscopic

Correspondence to: H.-W. Wang (hongwen@cycu.edu.tw).
Contract grant sponsor: National Science Council of the Republic of China; contract grant number: 95-2113-M-033-002.

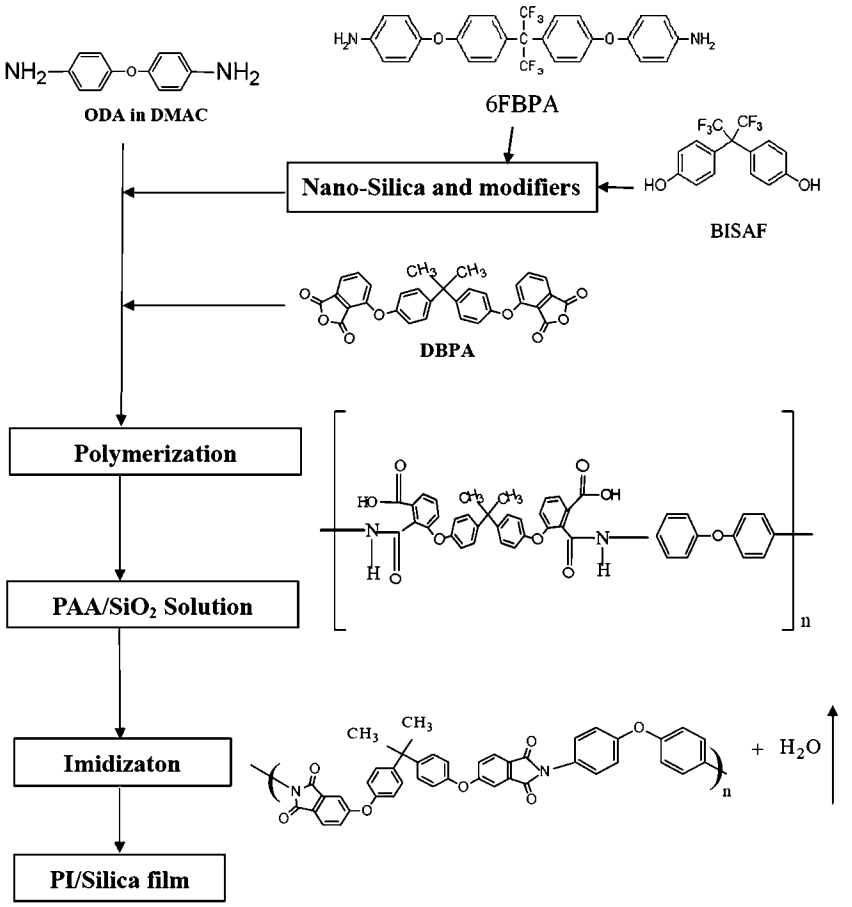

Figure 1 Reaction scheme of the PI–silica nanocomposites.

responses.[33–37] Different segmental mobilities have been observed; close to the filler surface, segmental relaxation times are significantly longer than those of an unfilled polymer.[33–35] Dynamic mechanical studies on nanofilled systems have indicated the presence of a separate relaxation event, which has been attributed to these less mobile chains within the interfacial region. A slow process, corresponding presumably to restricted mobility adjacent to the filler surface, has been identified, whereas the bulk polymer retains the normal segmental dynamics.[33–39] However, the performances of different nanocomposite systems are difficult to compare, and the same filler may produce different effects in different matrices or even in the same matrix under different processing conditions.[40–42] For example, the mechanical properties of epoxy matrices are enhanced by the use of surface-functionalized silica nanoparticles as reinforcing agents.[43] On the other hand, untreated silica nanoparticles appear to degrade the thermal properties in epoxy matrices, mainly because of the presence of residual moisture and organics.[44]

Many works on low-*k* nanocomposites focus on developing new types of monomers, increasing the free volume or porosity within the polymer matrix, or adding nanofillers (silica or clays) to polymer matrices. In this study, a novel process was used to synthesize PI–silica nanocomposites: the surface of the filler, silica nanoparticles, was modified with a fluorinated monomer before its incorporation into the PI matrix. Much cheaper nonfluorinated monomers such as 4,4′-oxydianiline (ODA or $C_{12}H_{12}N_2O$) and 4,4′-(4,4′-isopropylidenediphenoxy)bis(phthalic anhydride) (DBPA or $C_{31}H_{20}O_8$) for the PI matrix were used. ODA–DBPA has a typical *k* value of 3.2–3.4. The effects of untreated silica and fluorine-modified nanosilica fillers on the thermal, mechanical, and dielectric properties of PI–silica nanocomposites were investigated.

EXPERIMENTAL

Materials

Nanosilica colloid #4720 (purity ≅ 99.9%, size ≅ 17 nm), derived from tetraethoxysaline (TEOS) with a sol–gel process, was provided by Chang-Chun Petroleum Corp. (Taiwan). ODA (Aldrich, St. Louis, MO; 97%) and DBPA (Aldrich; 97%) were used as starting precursors for the PI matrix. *N*,*N*-Dimethylacetamide

(DMAc; Tedia, Fairfield, OH; 99%) was used as a solvent. 4″,4‴-(Hexafluoroisopropylidene)bis(4-phenoxyaniline) (6FBPA; Aldrich; 97%) and 4,4′-(hexafluoroisopropylindene)diphenol (BISAF; Aldrich; 97%) were employed as modifiers to modify the surface of the silica nanoparticles. The reaction scheme and the structures of all the chemicals used to form the PI–silica nanocomposites are shown in Figure 1.

Preparation of the PI films with silica

PI films with 3, 5, 10, or 15 wt % silica nanoparticles were prepared as follows. First, the desired silica colloids and 3 g of DMAc were mixed and stirred for 15 min (beaker A). Second, 1 nmol of the diamine (ODA) was dissolved in 1.5 g of DMAc and stirred for 15 min (beaker B). Then, the solutions in beakers A and B were mixed while stirring was continued for 24 h. Third, 1 nmol of the dianhydride (DBPA) was dissolved in 1.5 g of DMAc and stirred for 15 min (beaker C). The contents of beaker C were put into the mixture of beakers A and B and stirred for 24 h. The nanocomposite films were prepared by the casting of 3 mL of the final mixture solution onto a piece of a 50 mm $\times$ 50 mm glass slide. The resultant films were dried in an oven and subsequently imidized at a high temperature in air. An imidization program, such as heating from room temperature to 80°C in 30 min, heating at 80°C for 2 h, heating from 80 to 200°C in 5 h, heating from 200 to 300°C in 2 h, heating at 300°C for 45 min, and then cooling to room temperature, was employed.

Preparation of PI with fluorinated-monomer-modified silica

PIs with and without 15 wt % silica were chosen for further studies. Various amounts of 6FBPA or BISAF (1, 3, 5, or 10 wt % with respect to the PI weight) were added to the silica colloid (in 3 g of DMAc) and stirred for 15 min (beaker A). For PI without silica, only 6FBPA was stirred for 15 min. One nanomole of the diamine (ODA) was dissolved in 1.5 g of DMAc and stirred for 15 min (beaker B). Then, the contents of beakers A and B were mixed and stirred for 24 h. Finally, 1 nmol of the dianhydride (DBPA) was dissolved in 1.5 g of DMAc and stirred for 15 min (beaker C). The mixture of beaker C was put into the contents of beakers A and B and stirred for 24 h. The nanocomposite films were prepared and cured via the same procedure as the PI–silica films mentioned previously. The PIs with 15 wt % 6FBPA-modified silica are called the PI–15% SiO_2–F series, whereas those incorporated with BISAF-modified silica are called the PI–15% SiO_2–B series. PI–15% SiO_2–10% F means that the PI polymer matrix was incorporated with 15 wt % SiO_2 nanoparticles, whose surface was modified by 10 wt % 6FBPA.

Characterization of the nanocomposites

To reveal the distribution of silica nanoparticles in the PI matrix, transmission electron microscopy (TEM) was performed. The samples for the TEM study were taken from a microtomed section of the PI–silica nanocomposites, about 75 $\pm$ 15 nm thick, which were mounted in an epoxy resin. A JEOL (Tokyo, Japan) 200FX transmission electron microscope with an acceleration voltage of 120 kV was employed for the observations. Fourier transform infrared (FTIR) spectra were carried out with a Bio-Rad (Cambridge, MA) FTS-7 FTIR system at a resolution of 4.0 cm^{-1} ranging from 400 to 4000 cm^{-1} at room temperature. Thermogravimetric analysis (TGA) and differential scanning calorimetry (DSC) were performed to determine the thermal stability of the specimens. A Mettler–Toledo TGA/SDTA851 thermal analysis system was employed for the TGA experiments in air at a heating rate of 10°C/min from room temperature to 900°C. DSC was performed on a PerkinElmer (Wellesley, MA) DSC-7 differential scanning calorimeter at a heating/cooling rate of 10°C/min in a nitrogen atmosphere. The glass-transition temperatures (T_g) of the studied materials were recorded during the second scan with a calibration accuracy less than $\pm$0.3°C.

Dielectric parameters such as the capacitance and dissipation factor (tan δ) were measured with an Agilent (Santa Clara, CA) 4284A automatic component analyzer at various frequencies (10^2–10^6 Hz) in the temperature range of 30–150°C. A vacuum-evaporated gold electrode was deposited on both sides of the nanocomposite film (1.6 cm in diameter). The

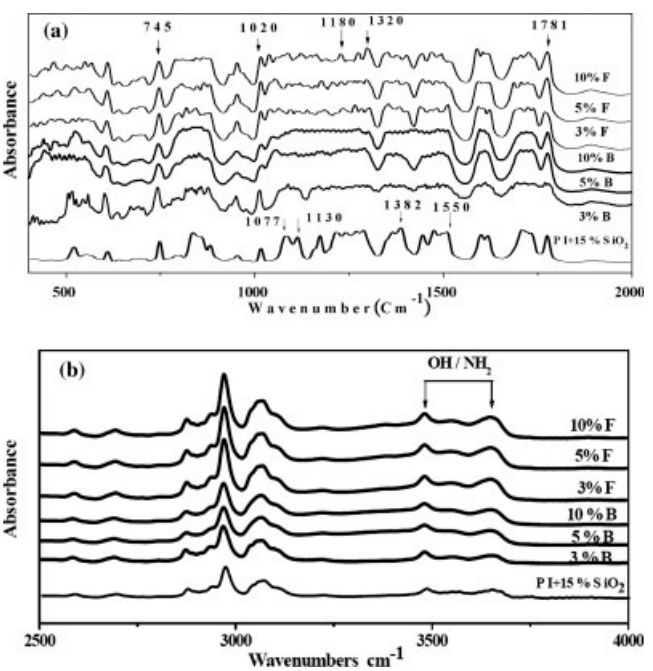

Figure 2 FTIR spectra for PI–15% SiO_2 and its nanocomposite series with modifiers 6FBPA (F) and BISAF (B).

TABLE I
Assignment of the IR Absorption Peaks to the Corresponding Vibration Modes

Frequency	Source	Assignment
745	PI	Imide ring
1020	SiO_2	Si—OH
1077 and 1130	SiO_2	O—Si—O
1180 and 1320	6FBPA and BISAF	$C—F_3$
1377 and 1382	PI	C—N
1550	PI	C=C
1720 and 1781	PI	Asymmetric/symmetric imide C=O stretching

thickness of the samples was 110 ± 5 μm. The k values of the specimens were calculated with the following equation: $C = k\varepsilon_0(A/d)$, where ε_0 is the vacuum permittivity (8.85×10^{-12} F/m), C is the capacitance (F), A is the electrode area, and d is the thickness of the specimen.

RESULTS AND DISCUSSION

FTIR

In this study, ODA and DBPA were used for the PI matrix. 6FBPA and BISAF were used to modify the surface of the silica nanoparticles. It was expected that the fluorinated precursors would reside close to the surface of the silica and modify the moiety of the PI–silica interface. Figure 2(a) shows the FTIR spectra below 2000 cm^{-1} for PI–15% SiO_2, PI–15% SiO_2–F, and PI–15% SiO_2–B series nanocomposites. The characteristic vibration bands of PI at 745 (imide ring), 1382 (C—N), 1550 (aromatic C=C), 1720 (C=O asymmetric stretching), and 1781 cm^{-1} (C=O symmetric stretch-

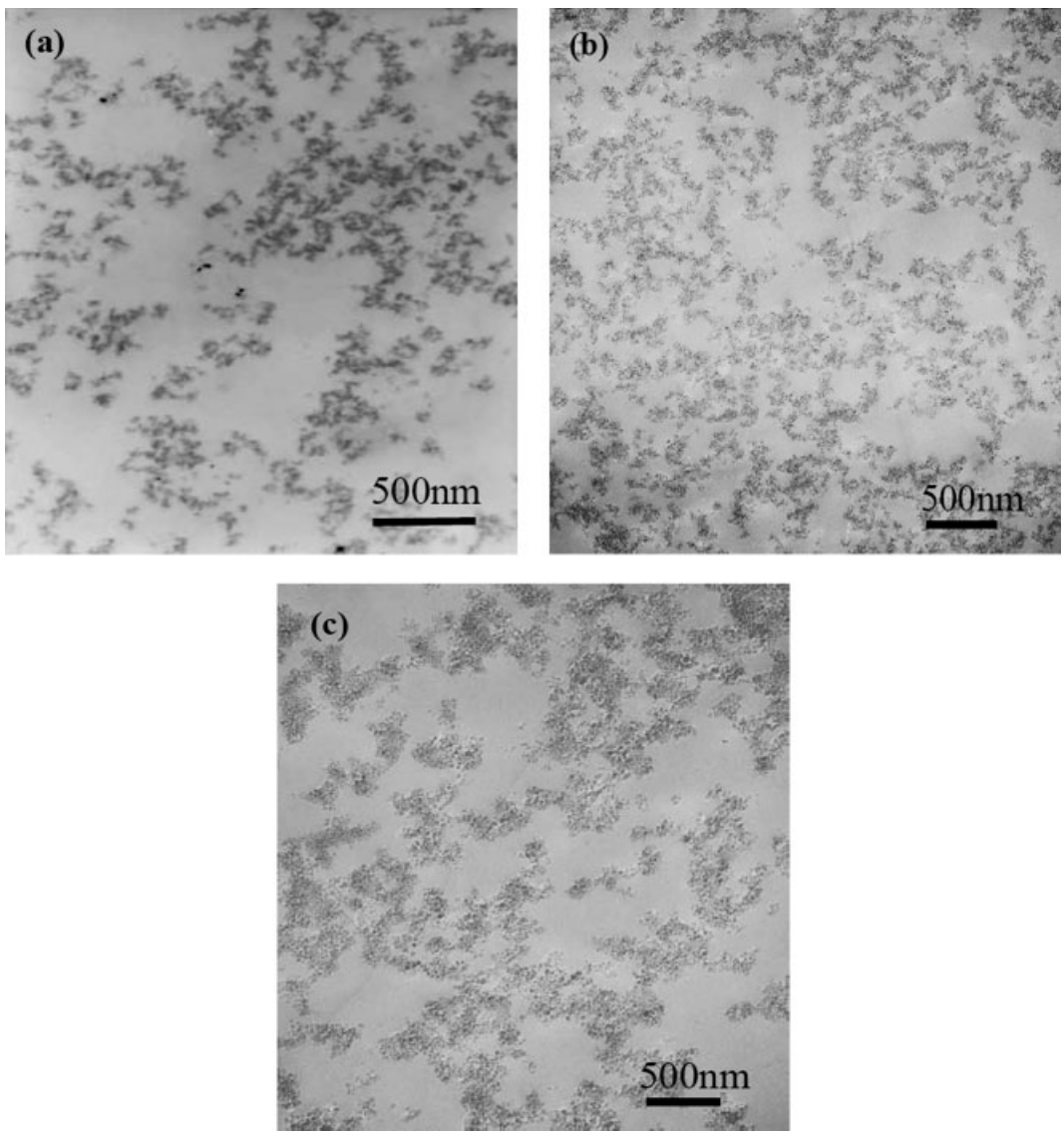

Figure 3 TEM micrographs for (a) PI–5% SiO_2, (b) PI–15% SiO_2–10% F, and (c) PI–15% SiO_2–10% B nanocomposites. PI–15% SiO_2–10% F exhibits a more uniform distribution of silica nanoparticles than the other two cases.

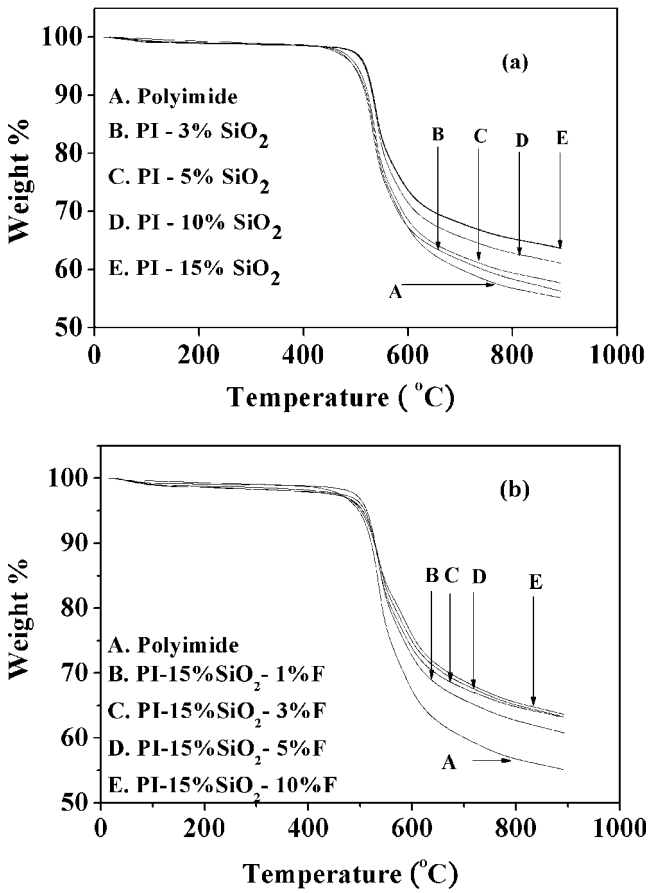

Figure 4 TGA curves for (a) PIs with silica and (b) PIs with modifier 6FBPA on 15% silica.

ing) are identified.[45–47] The characteristic absorption bands of the silica network Si—O—Si can also be observed at 1130 (Si—O—Si, asymmetric stretching) and 1077 cm^{-1} (Si—O—Si, vibration). Silanol stretching (Si—OH), which occurs at 1020 cm^{-1}, can also be observed for this hybrid material. Table I summarizes the assignments of the absorption peaks. These adsorption peaks for silica suggest that the main structures for the TEOS-derived silica are condensed species, followed to a smaller extent by the open-chain structure of silanol groups at the interface moiety. The PI–silica hybrid composites were successfully obtained, and the open-chain structure of the silanol groups may have existed in the interface of the silica and PI. The peaks at 1180–1320 cm^{-1} originated from the CF_3 group,[26] which is evident for the PI–15% SiO_2–F series but not very clear for the PI–15% SiO_2–B series. The ambiguous absorption peaks of CF_3 for the PI–15% SiO_2–B series may be attributed to the sampling of heterogeneous specimens (series B, as shown in the TEM micrographs). The distribution of CF_3 may not be uniform in the PI–15% SiO_2–B series.

The IR spectra over 2500 cm^{-1} are shown in Figure 2(b), in which O—H and N—H bonds at 3200–3500 cm^{-1} are indicated.[48] For the PI–15% SiO_2–F nanocomposites, N—H bands in the composite appearing at 3400–3600 cm^{-1} are stronger than those of PI–15% SiO_2–B nanocomposites. This might be related to the terminal amino groups (—NH_2; especially the modifier 6FBPA), which react with silica as well as the PI matrix to form new bonds. It is thought that 6FBPA not only is physically mixed but also exhibits stronger anchorage between. The end-cap amine group of 6FBPA is partially electropositively charged because of hydrogen bonding; an electrostatic attraction is expected when the liquid is removed.[49] In addition, 6FBPA is one of the chemical ingredients for PI polymerization and will give other bonding. That is, 6BFPA on the surface of silica will be dual-functioning: one function is to stabilize silica colloids, and the other is to provide chemical interactions with surrounding poly(amic acid) to form and integrate the final PI matrix. However, the BISAF modifier is not able to provide such dual functionality because its OH groups

TABLE II
Thermal Properties of the PI–Silica Nanocomposites

Sample	SiO_2 content	Modifier content	T_d (°C)[a]	T_g (°C)[b]	T_g (°C) from tan δ[c]
PI	0%	0%	494.4	219.9	236.2
PI–3% SiO_2	3%	0%	499.1	—	—
PI–5% SiO_2	5%	0%	501.4	—	—
PI–10% SiO_2	10%	0%	504.2	—	—
PI–15% SiO_2	15%	0%	508.3	220.2	237.2
PI–15% SiO_2–1% F	15%	1% 6FBPA	508.2	221.5	238.5
PI–15% SiO_2–3% F	15%	3% 6FBPA	511.2	222.7	239.4
PI–15% SiO_2–5% F	15%	5% 6FBPA	512.8	223.5	241.3
PI–15% SiO_2–10% F	15%	10% 6FBPA	509.5	224.9	245.5
PI–15% SiO_2–3% B	15%	3% BISAF	509.4	—	—
PI–15% SiO_2–5% B	15%	5% BISAF	511.2	—	—
PI–15% SiO_2–10% B	15%	10% BISAF	512.5	222.3	241.5

[a] Data obtained from TGA.
[b] Data obtained from DSC.
[c] Data obtained from DMA.

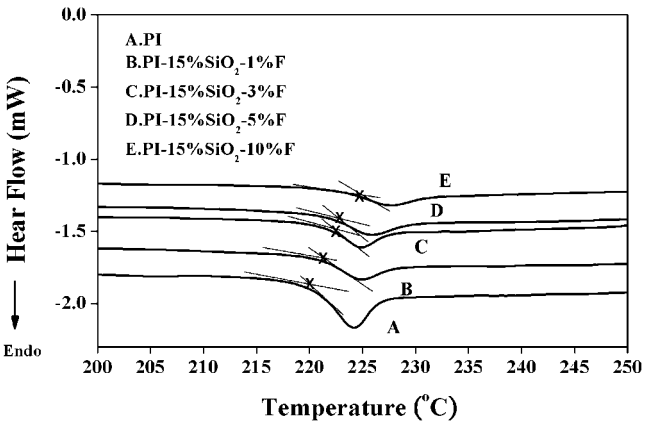

Figure 5 DSC for pristine PI and PI with 15% silica nanoparticles modified with fluorinated precursor 6FBPA.

have no reaction with the PI matrix but may form only hydrogen bonds with silica.

TEM

Figure 3(a–c) shows TEM micrographs for the PI nanocomposites incorporated with (a) 5 wt % silica, (b) 15 wt % silica modified by 10 wt % 6FBPA, and (c) 15 wt % silica modified by 10 wt % BISAF, respectively. The light regions represent the PI matrix, and the gray, dark spots correspond to the SiO_2 nanoparticles. The distribution of silica nanoparticles in Figure 3(b) is more uniform than that in Figure 3(a,c). That is, 6FBPA-modified silica nanoparticles distribute more uniformly in the PI matrix than the pristine silica and the BISAF-modified silica. In particular, the PI nanocomposite with BISAF-modified silica, as shown in Figure 3(c), contains a large flocculated area. From the TEM observations, the particle size of silica is estimated to be less than 20 nm, as expected from the supplier's specifications. It is thought that the modifier plays an important role in the uniformity of the silica distribution. As discussed in the last section, the 6FBPA modifier provides dual functionality for the nanocomposites, whereas the BISAF modifier reacts only with silica nanoparticles. The TEM images shown in Figure 3(b,c) demonstrate the differences in the uniformity.

Thermal and mechanical properties

The thermal decomposition behaviors of the PI–SiO_2 series (without modifiers) are presented in Figure 4(a), and those of the PI–15% SiO_2–F series are presented in Figure 4(b). In Figure 4(a), the onset of the decomposition temperature (T_d) of the PI–SiO_2 materials (curves B–E) is higher than that of pristine PI and shifts toward higher temperatures as the amount of SiO_2 is increased. The values of T_d for curves A–E in Figure 4(a) are approximately 494.4, 499.1, 501.4, 504.2, and 508.3°C, respectively. T_d of PI–15% SiO_2 is nearly 14°C higher than that of pristine PI. It is clear that the thermal stabilities of PI are enhanced by the incorporation of silica nanoparticles. However, T_d of the PI–15% SiO_2–F series seems to vary only slightly, as shown in curves B–E of Figure 4(b); the T_d values are 508.2, 511.2, 512.8, and 509.5°C, respectively. Table II sum-

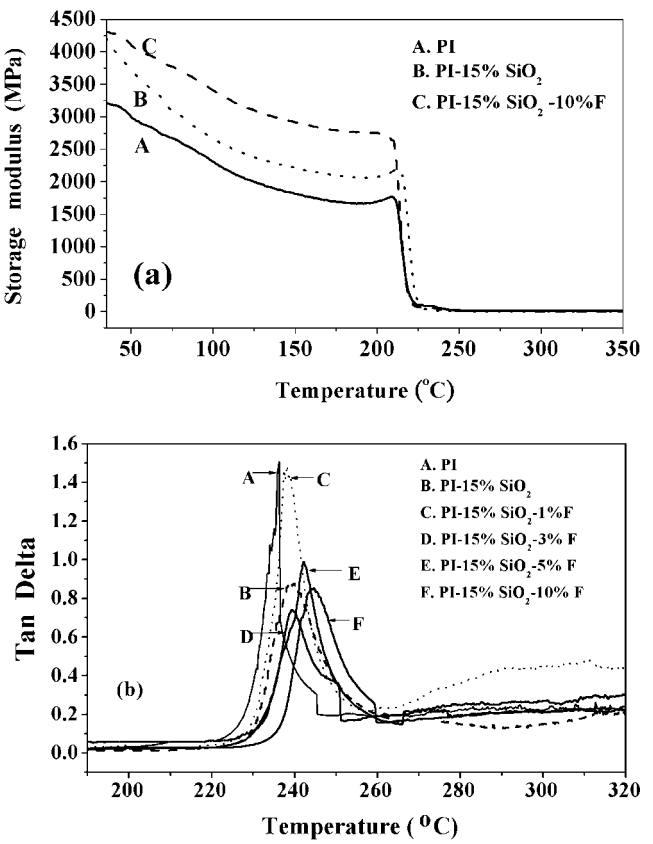

Figure 6 DMA tests for PI and PI–15% SiO_2–F series nanocomposites: (a) the storage modulus and (b) tan δ.

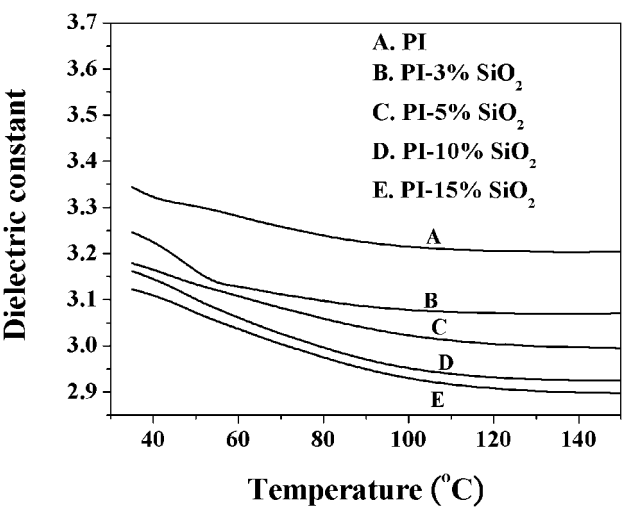

Figure 7 k values of the PI–silica hybrids without surface modification on silica at 1 MHz.

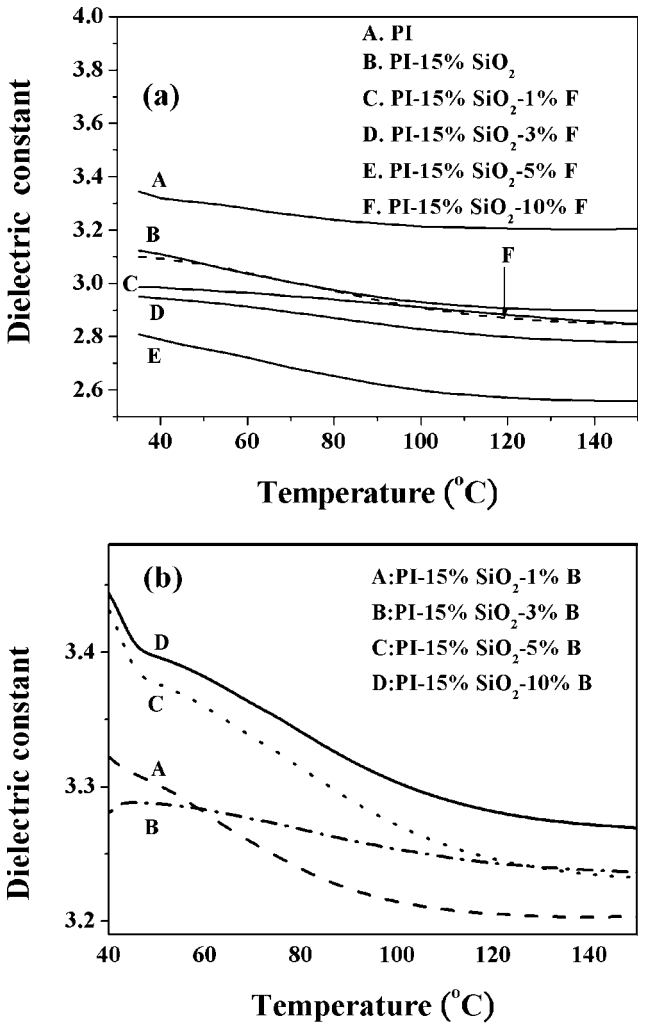

Figure 8 k values at 1 MHz for (a) PI and the PI–15% SiO_2–F series and (b) the PI–15% SiO_2–B series.

marizes the T_d values for the PI–15% SiO_2–F series and the PI–15% SiO_2–B series; they are only gently increased as the amount of the modifier increases. Modifiers 6FBPA and BISAF on the surface of silica seem to affect T_d of PI–15% SiO_2 insignificantly.

DSC thermograms for pristine PI and the PI–15% SiO_2–F series are shown in Figure 5. Pristine PI exhibits an endothermic peak at approximately 219.9°C, corresponding to its T_g. The T_g values shown in Figure 5 are approximately 219.9, 221.5, 222.7, 223.5, and 224.9°C for curves A–E, respectively. Increases in T_g due to the addition of modifier 6FBPA can be observed. The increment is significant and larger than the experimental deviation of ±0.3°C. The T_g values of the PI–15% SiO_2–F and PI–15% SiO_2–B nanocomposites obtained with DSC and dynamic mechanical analysis (DMA) techniques are tabulated in Table II. Both techniques demonstrate that T_g is enhanced by the addition of modifiers, but not the silica nanoparticles. That is, T_g of PI–15% SiO_2 seems insignificantly different from that of pristine PI, as shown in Table II. In Figure 6(a), the storage modulus of PI–15% SiO_2–10% F is clearly much higher than those of PI and PI–15% SiO_2. In Figure 6(b), broad peaks similar to those of the literature[35] above the tan δ peak can also be observed. Noticeably, the addition of the 6FBPA modifier causes a significant shift of T_g to higher temperatures. The modification on the surface of the silica nanoparticles exerts a considerable impact on T_g as well as the mechanical properties for the nanocomposites. It is thought that the restricted mobility of the polymer at the silica–polymer interface is largely responsible for this enhancement.[33–39]

Dielectric properties

As shown in Figure 7, k of pristine PI (ODA–DBPA) is around 3.2–3.4 at 1 MHz and slightly decreases as the temperature increases. As the amount of nanosilica in the PI matrix increases, the nanocomposite materials

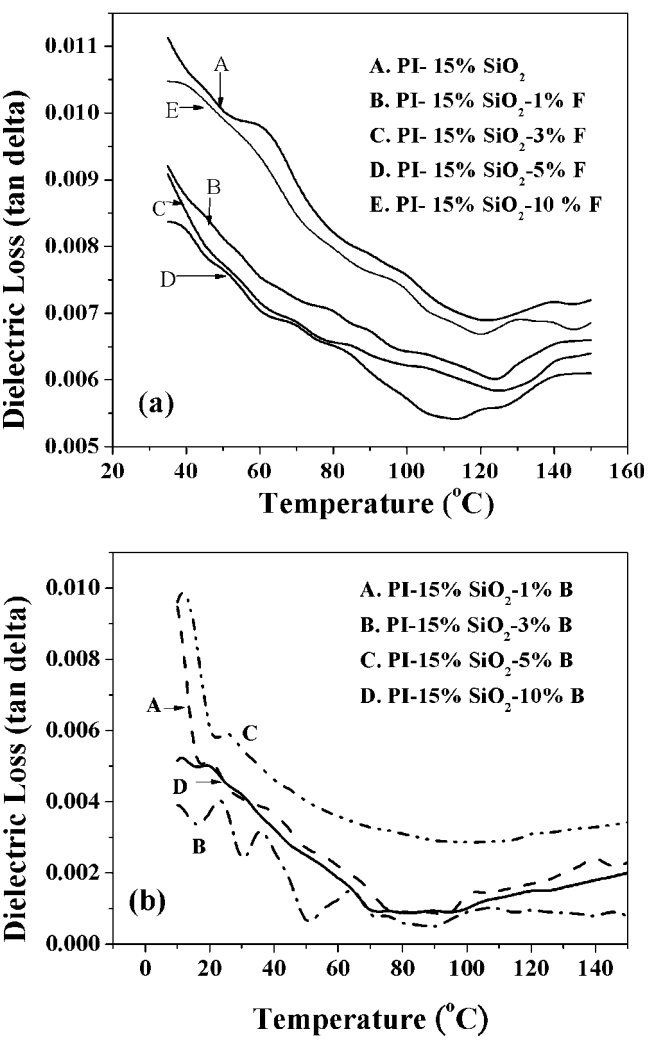

Figure 9 Dielectric loss of the PI–silica nanocomposites at 1 MHz. The silica nanoparticles were modified by (a) 6FBPA and (b) BISAF.

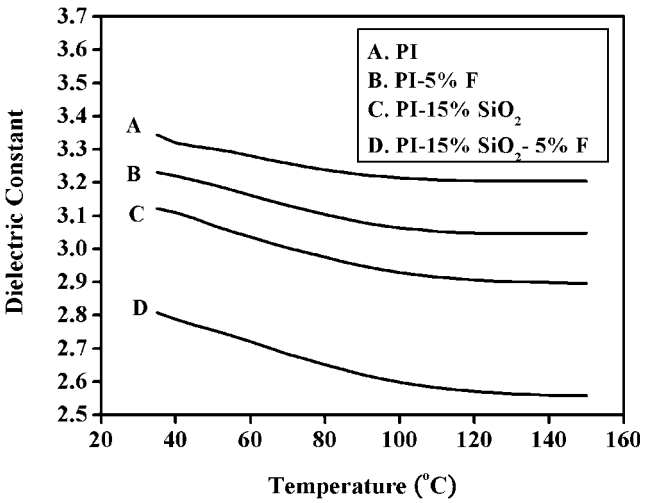

Figure 10 *k* values of PI and PI–silica nanocomposites: (A) pristine PI, (B) PI with 5% 6FBPA (without silica nanoparticles), (C) PI–15% SiO_2 (without modifier 6FBPA), and (D) PI–15% SiO_2 with 5% 6FBPA. The *k* values were measured at 1 MHz.

show a decrease in *k* to less than 2.9 (for 15 wt % SiO_2) at a high temperature. The decrease in *k* might be attributed to the large interfacial area and imperfection induced by the addition of silica nanoparticles. Figure 8(a) shows the *k* values for the PI–15% SiO_2–F series. A further reduction of *k* due to the addition of 6FBPA can be observed. The *k* values of the PI–15% SiO_2–F series are in the range of 3.1–2.55 and decrease as the amount of 6FBPA increases from 1 to 5 wt %. However, when the amount of 6FBPA increases up to 10 wt %, *k* slightly goes back to higher values of 3.1–2.9. This is an additional complex and might be related to the quality of the film specimen. The film specimens made from 10 wt % modifiers become more rigid and darker, and the homogeneities and roughness of the films become poor because of the addition of excess modifiers. The *k* values for the PI–15% SiO_2–B series are in the range of 3.45–3.2, which is slightly higher than that of pristine PI, as shown in Figure 8(b). No reduction of *k* can be observed. The dielectric losses of the PI–15% SiO_2–F series and the PI–15% SiO_2–B series versus the temperature are shown in Figure 9(a,b), respectively, and are reasonably low for applications. For the PI–15% SiO_2–F series, the dielectric loss also decreases as the fluorine content increases, except for the case of 10 wt % 6FBPA. This corresponds to the increase in *k* and the excess dianiline in this particular case. For the PI–15% SiO_2–B series, the dielectric losses are low but have no clear trend with the addition of BISAF. Figure 10 clearly compares the *k* values for four typical specimens, that is, PI, PI–5% F (i.e., no silica), PI–15% SiO_2, and PI–15% SiO_2–5% F. It demonstrates that the coexistence of 5 wt % 6FBPA and 15 wt % silica makes the nonfluorinated PI (ODA–DBPA) materials very attractive for low-*k* applications.

In this study, a novel modified process used to achieve low *k* values comparable to those of expensive fluorinated PI materials has been demonstrated. The novel mixing of 6FBPA-modified silica nanoparticles into PI materials has the merits of low consumption of the fluorinated starting monomers and low *k* values. The reduction of *k* for PI materials via the incorporation of silica colloids is attributed to the additional interfaces between the silica and PI materials. It is believed that the nanoparticles will result in more imperfections or free volumes by introducing uniformly distributed interfaces. Silica has a higher *k* value (3.8–4.0) than PI materials. The addition of silica should generally lead to higher *k* values. This is true for bulk silica particles. However, the surface area becomes significant when the particle diameter is less than 20 nm (ratio of the surface area to the volume = 0.3 nm^{-1}). In our case, silica nanoparticles with diameters around 17 nm have been used. The interface between the silica and PI matrix, where silanol groups exist, gives the opportunity of free volume at the surface of the modified silica nanoparticles. However, the inhomogeneity of the composites will adversely influence the symmetric polarization degree of the molecules in the composites and thus the dielectric properties. From the dielectric values listed in Figure 8, it seems that more fluorine may not ensure a lower *k* value. The modifier BISAF possesses a higher fluorine content than 6FBPA but does not reduce *k*. The uniformity of fluorine-modified silica nanoparticles plays an important role in the reduction of *k*. The reduced *k* values in this study are likely controlled by a free-volume mechanism (i.e., the imperfection of the silica–polymer interface) rather than the symmetric fluorinated groups.

CONCLUSIONS

A series of PI–silica nanocomposites have been synthesized by the mixing and polymerization of novel fluorine-modified silica nanoparticles in a PI matrix. With silica or 6FBPA-modified silica nanoparticles, the *k* values of the PI films are greatly reduced. The modifier 6FBPA provides dual functions in the formation of uniform PI–SiO_2 nanocomposites. The modifier BISAF possesses a higher fluorine content than 6FBPA but does not significantly affect *k* because of the flocculation of silica. It is believed that the free volume originating from the imperfection of the interface between PI and silica, when distributed uniformly, makes a significant contribution to the reduction of *k*.

References

1. Martin, S. J.; Godschalx, J. P.; Mills, M. E.; Shaffer, E. O., II; Townsend, P. H. Adv Mater 2000, 12, 1769.

2. Treichel, H.; Goonetilleke, C. Adv Eng Mater 2001, 7, 461.
3. Lim, O. K.; Lee, J. I.; Kim, Y. J.; Park, J. Y. Micro Opt Technol Lett 2004, 40, 177.
4. Wilson, D.; Stenzenberger, H. D.; Hergenrother, P. M. Polyimides; Chapman & Hall: London, 1990.
5. Ghosh, M. K.; Mittal, K. L. Polyimides: Fundamentals and Applications; Marcel Dekker: New York, 1996.
6. St. Clair, A. K.; St. Clair, T. L.; Winfree, W. P. U.S. Pat. 5,338,826 (1994).
7. Hougham, G.; Tesoro, G.; Shaw, J. Macromolecules 1994, 27, 3642.
8. Hougham, G.; Tesoro, G.; Viehbeck, A. Macromolecules 1996, 29, 3453.
9. Hougham, G.; Tesoro, G.; Viehbeck, A.; Chapplesokol, J. D. Macromolecules 1994, 27, 5964.
10. Simposon, J. O.; St. Clair, A. K. Thin Solid Films 1997, 308, 480.
11. Ukishima, S.; Ijijma, M.; Masatoshi, S.; Takahashi, Y.; Fukada, E. Thin Solid Films 1997, 308, 475.
12. Liang, T.; Makita, Y.; Kimura, S. Polymer 2001, 42, 4867.
13. Lee, C.; Shul, Y.; Han, H. J Polym Sci Part B: Polym Phys 2002, 40, 2190.
14. Alegaonkar, P. S.; Mandale, A. B.; Sainkar, S. R.; Bhoraskar, V. N. Nucl Instrum Methods Phys Res B 2002, 194, 281.
15. Goto, K.; Akiike, T.; Inoue, Y.; Matsubara, M. Macromol Symp 2003, 199, 321.
16. Vora, R. H.; Krishnan, P. S. G.; Goh, S. H.; Chung, T. S. Adv Funct Mater 2001, 11, 361.
17. Wang, W. C.; Vora, R. H.; Kang, E. T.; Neoh, K. G.; Ong, C. K.; Chen, L. F. Adv Mater 2004, 16, 54.
18. Chen, Y. W.; Wang, W. C.; Yu, W. H.; Yuan, Z. L.; Kang, E. T.; Neoh, K. G.; Krauter, B.; Greiner, A. Adv Funct Mater 2004, 14, 471.
19. Chen, Y. W.; Wang, W. C.; Yu, W. H.; Kang, E. T.; Neoh, K. G.; Vora, R. H.; Ong, C. K.; Chen, L. F. J Mater Chem 2004, 14, 1406.
20. Hedrick, J. L.; Carter, K. R.; Richter, R.; Miller, R. D.; Russell, T. P.; Flores, V. Chem Mater 1998, 10, 39.
21. Charlier, Y.; Hedrick, J. L.; Russell, T. P. Polymer 1995, 36, 4529.
22. Hedrick, J. L.; Russell, T. P.; Sanchez, M.; Dipietro, R.; Swanson, S. Macromolecules 1996, 29, 3642.
23. Kramarenko, V. Y.; Shantalil, T. A.; Karpova, I. L.; Dragan, K. S.; Privalko, E. G.; Privalko, V. P.; Fragiadakis, D.; Pissis, P. Polym Adv Technol 2004, 15, 144.
24. Bershtein, V. A.; Egorova, L. M.; Yakushev, P. N.; Pissis, P.; Sysel, P.; Brozova, L. J Polym Sci Part B: Polym Phys 2002, 40, 1056.
25. Tsai, M. H.; Whang, W. T. Polymer 2001, 42, 4197.
26. Yen, C. T.; Chen, W. C.; Liaw, D. J.; Lu, H. Y. Polymer 2003, 44, 7079.
27. Leu, C. M.; Chang, Y. T.; Wei, K. H. Chem Mater 2003, 15, 3721.
28. Lin, W. J.; Chen, W. C. Polym Int 2004, 53, 1245.
29. Hedrick, J. L.; Cha, H. J.; Miller, R. D.; Yoon, D. Y.; Brown, H. R.; Srinivasan, S.; Pietro, R. D. Macromolecules 1997, 30, 8512.
30. Liu, W. C.; Yang, C. C.; Chen, W. C.; Dai, B. T.; Tsai, M. S. J Non-Cryst Solid 2002, 311, 233.
31. Jiang, L. Y.; Leu, C. M.; Wei, K. H. Adv Mater 2002, 14, 426.
32. Ahmad, Z.; Mark, J. E. Chem Mater 2001, 13, 3320.
33. Arrighi, V.; Higgins, J. S.; Burgess, A. N.; Floudas, G. Polymer 1998, 39, 6369.
34. Gagliardi, S.; Arrighi, V.; Ferguson, R.; Telling, M. T. F. Phys B 2001, 301, 110.
35. Arrighia, V.; McEwena, I. J.; Qiana, H.; Serrano Prietob, M. B. Polymer 2003, 44, 6259.
36. Tsagaropoulos, G.; Eisenberg, A. Macromolecules 1995, 28, 396.
37. Tsagaropoulos, G.; Eisenberg, A. Macromolecules 1995, 28, 6067.
38. Yim, A.; Chahal, R. S.; St Pierre, L. E. J Colloid Interface Sci 1973, 43, 583.
39. Yano, S.; Furukawa, T.; Kodomari, M.; Kurita, K. Kobunshi Ronbunshu 1996, 53, 218.
40. Huang, Y.; Jiang, S.; Wu, L.; Hua, Y. Polym Test 2004, 23, 9.
41. Beloqui, B. J.; Fernandez-Gracia, J. C.; Orgiles-Barcelo, A. C.; Mahiques-Bugiada, M. M.; Martin-Martinez, J. M. J Adhes Sci Technol 1999, 13, 695.
42. Preghenella, M.; Pegoretti, A.; Migliaresi, C. Polymer 2005, 46, 12065.
43. Kang, S.; Hong, S. I.; Choe, C. R.; Park, M.; Rim, S.; Kim, J. Polymer 2001, 42, 879.
44. Sun, Y.; Zhang, Z.; Moon, K.; Wong, C. P. J Polym Sci Part B: Polym Phys 2004, 42, 3849.
45. Wang, Y. W.; Yen, C. T.; Chen, W. C. Polymer 2005, 46, 6959.
46. Lee, J. H.; Im, J. S.; Song, K. W.; Lee, J. O.; Yoshinaga, K. J Macromol Sci 2004, 41, 1345.
47. Qiu, F. X.; Zhou, Y. M.; Liu, J. Z. Eur Polym J 2004, 40, 713.
48. Lee, Y. J.; Huang, J. M.; Kuo, S. W.; Lu, J. S.; Chang, F. C. Polymer 2005, 46, 173.
49. Leu, C. M.; Wu, Z. W.; Wei, K. H. Chem Mater 2002, 14, 3016.